Ab initio vibration–rotation-tunneling spectra and dynamics of $H_2 \cdot F^-$ and its isotopomers

A. I. Boldyrev and Jack Simons
Department of Chemistry, The University of Utah, Salt Lake City, Utah 84112

G. V. Mil'nikov
Institute of Structural Macrokinetics, Chernogolovka, Moscow Region 142432, Russia

V. A. Benderskii, S. Yu. Grebenshchikov, and E. V. Vetoshkin
Institute for Chemical Physics in Chernogolovka, Chernogolovka, Moscow Region 142432, Russia

(Received 1 August 1994; accepted 12 October 1994)

Ab initio computations of the potential energy surface (PES) of the ground electronic state of $H_2 \cdot F^-$ have been performed as a function of the stretching $F–H_2$ (R) and H_2 rotation (θ) coordinates. Minima on the PES correspond to linear $H–H–F^-$ structures, while the transition state is T-shaped. The F^- to H_2 distance increases in the transition state from 2.07 to 3.10 Å, demonstrating strong coupling between the θ and R degrees of freedom. The vibration–rotation-tunneling spectra are calculated by diagonalizing the five dimensional Hamiltonian matrix that describes free rotation of the triatomic (three coordinates) plus the internal θ and R motions. For total angular momentum $J=0$, the spacing between levels in the tunneling doublets increases from 0.029 to 6.74 cm^{-1} as the stretching quantum number n corresponding to R motion varies from 0 to 5. The splittings increase even more strongly with the bending quantum number. For $J=1$, each level in the tunneling doublets is further split by Coriolis forces. K-doubling is found to be an order of magnitude smaller than the tunneling splitting. In the symmetric isotopomers $D_2 \cdot F^-$ and $T_2 \cdot F^-$, the tunneling splitting drops by 3 and 4 orders of magnitude compared to $H_2 \cdot F^-$, and thus becomes comparable with the K-doubling for $J=1$. Finally, incoherent tunneling, appropriate to condensed phase environments, of the H_2F^- system is also treated. © *1995 American Institute of Physics.*

I. INTRODUCTION

Recently, the van der Waals complex of H_2 and F^- has received widespread attention due to the studies of Neumark and co-workers.[1] By studying the photoelectron spectra of $H_2 \cdot F^-$ they found that the geometry of the ground electronic state of this complex is close to that of the transition state for the collinear *neutral* $F+H_2$ reaction.

Earlier *ab initio* computations of the PES for $H_2 \cdot F^-$ had been carried out by Simons and co-workers.[2] Two symmetric minima, corresponding to linear HHF^- structures of the complex, were found. Because hindered rotation of the nearly rigid H_2 moiety occurs, $H_2 \cdot F^-$ is what Nesbitt and Naaman[3] called a ''pinwheel'' complex. However, unlike the cases considered in Ref. 3, the T-shape structure of $H_2 \cdot F^-$ is a transition state rather than an equilibrium geometry. The results of Simons and co-workers[2] indicated that hindered rotation is strongly coupled to interfragment oscillation of the $H_2 \cdot F^-$. In this respect, the H_2F^- complex provides a very relevant example involving two-dimensional (2D) tunneling. A distinctive feature of this complex is that hydrogen bonding provides potential barriers for hindered rotation that are very high, which produces long progressions of vibrational levels split by tunneling. Because the potential wells are deep and narrow, the nuclear wave functions for low-lying levels are well localized. Hence, at first glance, the concept of a single well defined ''equilibrium molecular structure,'' common in spectroscopy, seems applicable, at least for low-lying levels.

The concept of multidimensional nuclear tunneling attracted much attention in the early 1980s (see, for example, reviews in Refs. 4 and 5). This concept emphasizes that tunneling in many chemical systems can involve significant displacements along several coordinates (along and transverse to the reaction path). The transverse coordinates can actively promote (for symmetric coupling with the reactions coordinate) or suppress (for antisymmetric coupling) the tunneling.[6] In the coherent tunneling regime treated in Sec. IV, this influence manifests itself in the strong dependence of the tunneling splitting on the quantum numbers of the transverse modes.[7,8] In addition to the tunneling splitting, the geometry of the transition state also depends on the quantum numbers of the transverse modes.

The essential features of two dimensional coherent tunneling can be elucidated by numerical diagonalization of a Hamiltonian matrix. However, analysis of incoherent tunneling treated in Sec. IV requires approximate semiclassical methods, among which a multidimensional version of the so-called instanton technique is shown to be quite promising.[5]

The vibration–rotation-tunneling (VRT) spectra of many molecules have already been studied both experimentally, $(H_2O)_2$,[9] $(H_2O)_3$,[10] $(NH_3)_2$,[11] $(HF)_2$,[12] $(HCl)_2$,[13] $NH_3 \cdot H_2O$,[14] $NH_3 \cdot Ar$,[15] $C_2H_3^+$,[16] (and many others reviewed in Refs. 17) and theoretically, $(H_2O)_2$,[18] $(NH_3)_2$,[19] $(HF)_2$,[20] H_2He^+,[21] $C_2H_3^+$,[22] $LiBH_4$,[23] $LiCH_4^+$.[23] However we did not find any earlier experimental or theoretical study of the VRT spectra of the $H_2 \cdot F^-$ complex, which is expected to have substantial tunneling splittings.

In this paper, the $H_2 \cdot F^-$ complex is studied in both the coherent and incoherent regimes for which tunneling dynam-

TABLE I. Molecular parameters of the $H_2 \cdot F$- system.

Method	Linear E_{total} (a.u.)	H–H–F$^-$ R (Å)	r (Å)	θ(°)	$\omega_1(\sigma)$ (cm^{-1})	$\omega_2(\sigma)$ (cm^{-1})	$\omega_3(\pi)$ (cm^{-1})	$V^{\#}$ (cm^{-1})
MP2(full)[a]	−100.922 239	2.071	0.787	180.	3607	383	1004	
QCISD(T)[a]	−100.912 629	2.074	0.792	180.	3536	384	976	
CCSD(T)[b]	−100.905 480	2.075	0.770	180.				
Method	Angular E_{total} (a.u.)	$H_2 \cdot F^-$ R (Å)	r (Å)	θ(°)	$\omega_1(a_1)$ (cm^{-1})	$\omega_2(a_1)$ (cm^{-1})	$\omega_3^{\#}(b_2)$ (cm^{-1})	$V^{\#}$ (cm^{-1})
MP2(full)[a]	−100.911 147	3.099	0.736	90.	4531	87	$513i$	2434
QCISD(T)[a]	−100.901 087	2.988	0.742	90.	4407	103	$528i$	2533

[a]Using 6-311++G($2df$,$2pd$) basis set.
[b]Data from Ref. 2.

ics is the key feature. Microwave and far-infrared spectra, which commonly provide information on tunneling, are not yet available for this complex, but we hope the results of our calculations may guide experimentalists to these ends. The paper is organized as follows: In Sec. II the *ab initio* quantum chemical calculations of the PES are described. The topology of the PES is discussed in Sec. III. Section IV is devoted to detailing our procedure for calculating the vibration–rotation-tunneling spectra of $H_2 \cdot F^-$ and its $HD \cdot F^-$, $D_2 \cdot F^-$, $HT \cdot F^-$, $DT \cdot F^-$, and T_2F^- isotopomers in the coherent regime. In Sec. V, temperature dependent incoherent tunneling is considered, and in Sec. VI we provide an overview of our conclusion.

II. THE *AB INITIO* POTENTIAL ENERGY SURFACE

We first optimized the geometries of the stable linear H–H–F$^-$ and T-shaped transition state $H_2 \cdot F^-$ structures employing analytical gradients[24] within the GAUSSIAN 92 program[25] with polarized split-valence basis sets [6-311++G($2df$,$2pd$)] at the MP2(full) level. Then, we repeated the geometry optimization at a more sophisticated level of theory; the quadratic configuration interaction with single and double excitations and approximate incorporation of triple excitations[26] [QCISD(T)] method, using the same 6-311++G($2df$,$2pd$) basis sets.

At both levels of theory, the linear structure is found to be a global minimum and the T-structure is found to be a saddle point for the internal rotation of H_2. Our optimal geometric parameters and harmonic frequencies for these two structures are presented in Table I together with previous data for the linear structure obtained by Simons and co-workers.[2]

The MP2(full)/6-311++G($2df$,$2pd$) equilibrium geometries are very close to those obtained at the QCISD(T)/6-311++G($2df$,$2pd$) level and to the CCSD(T) data of Ref. 2. Therefore, the potential energy surface for our subsequent rotation–vibration-tunneling calculations was calculated at the MP2(full)/6-311++G($2df$,$2pd$) level. The PES for internal rotation of $H_2 \cdot F^-$ was calculated in the internal coordinates presented in Fig. 1, where r is the H–H bond length, R is a distance from the F$^-$ to the center of the H–H bond, and θ is the angle between R and r. Because the H–H bond length (r) changes only slightly from the global-minimum structure to the saddle point, and to reduce the number of internal coordinates from three to two, we optimized r for every R and θ and the resultant energies were used to build the PES. Energies at the MP2(full)/6-311++G($2df$,$2pd$) level were calculated for every R=(2.0, 1.9, 1.8, 1.7, 1.6, 1.5, 2.0705, 2.0770, 2.0965, 2.1261, 2.1630, 2.2520, 2.3619, 2.5132, 2.8803, 2.9634, 3.0336, 3.0817, and 3.0995 Å) and θ=(0°, 5°, 10°, 15°, 20°, 30°, 40°, 50°, 60°, 70°, 75°, 80°, 85°, and 90°) except at points where the energy was much higher than the internal rotation barrier's energy. The resultant number of points on the two-dimensional PES was 345 (the data are available on request from the authors).

III. TOPOLOGY OF THE POTENTIAL ENERGY SURFACE

Our calculations show that the H–H distance r remains nearly constant (near r_e=0.787 Å) throughout the range of θ and R variation. This fact and the high frequency of the H–H vibration in the $H_2 \cdot F^-$ complex (see Table I) is used to separate this vibration from the low frequencies describing the relative motions of H_2 with respect to F$^-$. Because the H_2 rotor is assumed to be "stiff," the potential energy surface (PES) can be considered as two dimensional $V=V(R,\theta)$, with R_e=2.071 Å corresponding to the equilibrium linear geometry of the complex. Such a PES describes the θ motion of a semirigid internal H_2 rotor coupled to the low-frequency $H_2 \cdot F^-$ vibration (R). It has minima at θ=0, and π, and a saddle point at $\theta=\pi/2$ (see Fig. 2). Computing the rovibrational spectra for this PES requires an analytical expression for V to use in the numerical diagonalization. Such an expression needs to reproduce the following features of the PES:

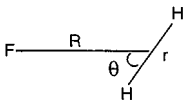

FIG. 1. Internal coordinates r, R, and θ used for the $H_2 \cdot F^-$.

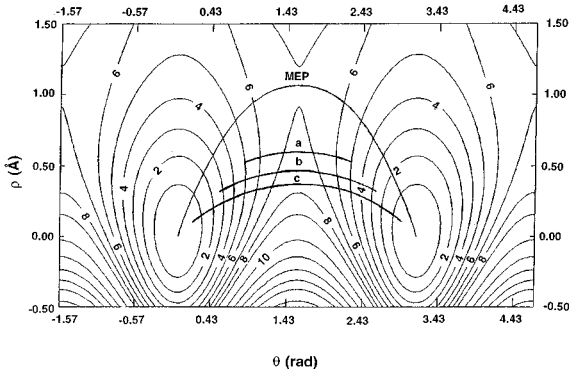

FIG. 2. Contour plot of the potential (1) (in kcal/mol) with the parameters from Table II for the $H_2 \cdot F^-$ complex. Minimum energy path and calculated instanton trajectories Eqs. (11) for temperatures $T=111$ K (a), 100 K (b), and 77 K (c) are shown.

(1) it has minima at $R=R_e$, $\theta_e=0$, π;
(2) it has a saddle point at $R=3.099$ Å [i.e., $\rho=(R-R_e)=1.028$ Å] and $\theta=\pi/2$;
(3) it should reproduce the barrier height $V^{\neq}$ at the saddle point;
(4) it should reproduce the *ab initio* vibrational frequencies at the equilibrium and saddle points.

A potential function that satisfies these conditions was constructed as a polynomial in the radial displacement coordinate $\rho=(R-R_e)$ (to facilitate the calculation of matrix elements using the harmonic oscillator basis set),

$$V(\rho)=V_0(\rho)+1/2V_2(\rho)(1-\cos 2\theta), \tag{1a}$$

where

$$V_0(\rho)=b_1\rho^2+b_2\rho^3+b_3\rho^4, \tag{1b}$$

$$V_2(\rho)=V_2+d_1\rho+d_2\rho^2+d_3\rho^3+d_4\rho^4, \tag{1c}$$

and the constants b_n, d_n, and V_n are given in Table II. The *ab initio* PES, is reproduced to within ~6% by this analytical function.

For the mixed isotopomers $HD \cdot F^-$, $HT \cdot F^-$, and $DT \cdot F^-$ the coordinate R as defined in Fig. 1 is no longer appropriate since the geometric center of the internal rigid rotor does not coincide with its center of mass. To preserve the form of the kinetic energy operator in the full Hamiltonian, two new coordinates must be used, one of which is the distance R_1 between the F nucleus and the center of mass of the internal rotor and the other is the angle θ_1 between R_1 and the rotor's internuclear axis. The old coordinates R, θ and new coordinates R_1 and θ_1 are related as follows:

$$R=(R_1^2+\delta^2-2R_1\delta\cos\theta_1)^{1/2}\approx R_1[1-(\delta/R_1)\cos\theta], \tag{2a}$$

$$\sin^2\theta=R_1^2\sin^2\theta_1(R_1^2+\delta^2-2R_1\delta\cos\theta_1)^{-1}$$
$$\approx\sin^2\theta_1[1+2(\delta/R_1)\cos\theta_1], \tag{2b}$$

where δ is the distance between the center of mass and the geometric center of the internal rotor,

$$\delta=r_e|m_1-m_2|[2(m_1+m_2)]^{-1}.$$

The approximate equalities given above result from expansion in powers of δ/R. This transformation makes the potential asymmetric with respect to $\theta=\pi/2$. Its analytical form can be easily derived from Eqs. (1), with the use of Eqs. (2). Note that since the distances between the center of mass and the geometric center of internal rotor is much smaller than R, the polynomial form of the potential in R and $\cos 2\theta$ is well preserved.

TABLE II. The Parameters of the analytical fit of the *ab initio* PES.

Parameter	Value	Parameter	Value
$\omega_2(\sigma)$ (cm^{-1}), H–H–F^-	357	b_1 (cm^{-3})	$3.428\,322\times10^{19}$
$\omega_3(\pi)$ (cm^{-1}), H–H–F^-	899	b_2 (cm^{-4})	$-2.497\,009\times10^{27}$
$\omega_2(a_1)$ (cm^{-1}), H_2F^-	81	b_3 (cm^{-5})	$5.115\,066\times10^{35}$
$\omega_3^{\#}(b_2)$ (cm^{-1}), H_2F^-	$458i$	d_1 (cm^{-2})	$-4.701\,781\times10^{11}$
$V^{\#}$ (cm^{-1})	2454	d_2 (cm^{-3})	$3.172\,015\times10^{19}$
V_{max} (cm^{-1})	3746	d_3 (cm^{-4})	$-1.741\,534\times10^{27}$
V_2 (cm^{-1})	$3.746\,36\times10^3$	d_4 (cm^{-5})	$5.366\,393\times10^{35}$

IV. SPECTRA

A. $H_2 \cdot F^-$; D_2F^-, T_2F^-

The methodology for accurate calculation of rovibrational levels of floppy molecules is well developed (see Refs. 17–23). The Hamiltonian for the three nuclei of a triatomic system is

$$H=\frac{\hbar^2}{2}\sum\frac{\nabla_i^2}{m_i}+V, \tag{3}$$

where ∇_i^2 is the Laplacian for the ith nucleus. A general approach for calculating the rovibration spectrum of the Hamiltonian (3) has already been developed in connection with H_2–rare gas van der Waals complexes and atom–diatom scattering (see, for example Ref. 27). The strategy, due to Eckart,[28] Curtiss *et al.*,[29] and Sutcliffe[30] is to first separate the translational motion from the kinetic energy operator, thus reducing to six the number of active variables. Then one makes an orthogonal transformation from space-fixed to body-fixed coordinates with the matrix of this transformation depending parametrically on three Euler angles α, β, γ that describe the overall rotation of the three-atom complex.[31] Because the potential V is independent of α, β, and γ, the Hamiltonian (3), with the center-of-mass motion removed, assumes the following form (the length of the stiff internal rotor is denoted ρ):

$$H=-\frac{\hbar^2}{2\mu_1\rho^2}\frac{\partial}{\partial\rho}\left(\rho^2\frac{\partial}{\partial\rho}\right)-\frac{\hbar^2}{2}\left(\frac{1}{\mu_1\rho^2}+\frac{1}{\mu_2 r_e^2}\right)\frac{1}{\sin\theta}\frac{\partial}{\partial\theta}\left(\sin\theta\frac{\partial}{\partial\theta}\right)+V(\cos\theta,\rho)+H_{VR}$$
$$\equiv H_0+H_{VR}, \tag{4}$$

where H_{VR} includes the rotational tumbling energy plus the vibration–rotation interaction, both of which depend on three Euler angles α, β, γ, and the polar angle θ of the internal

TABLE III. Energies (E, cm^{-1}) and tunneling splittings (Δ,cm^{-1}) of the vibration–rotation-tunneling states in $H_2 \cdot F^-$, $D_2 \cdot F^-$, and $T_2 \cdot F^-$ for the case $J=0$.

	$H_2 \cdot F^-$		$D_2 \cdot F^-$		$T_2 \cdot F^-$	
$(+/-,n,\nu)$	E	Δ	E	Δ	E	Δ
(+00)	983.273		720.657		599.861	
(−00)	983.302	0.029	720.657	0.000 047	599.861	0.000 001
(+10)	1297.162		963.300		809.892	
(−10)	1297.287	0.125	963.300	0.000 29	809.892	0.000 003
(+20)	1588.081		1195.314		1012.675	
(−20)	1588.495	0.414	1195.315	0.001 2	1012.675	0.000 01
(+30)	1850.048		1415.283		1207.484	
(−30)	1851.323	1.28	1415.287	0.004 4	1207.484	0.000 06
(+40)	2072.641		1621.232		1393.385	
(−40)	2076.317	3.68	1621.247	0.015	1393.386	0.000 21
(+02)	2275.635		1763.280		1487.892	
(−02)	2312.187	36.6	1763.475	0.20	1487.894	0.002 5
(+50)	2245.891		1810.218		1569.129	
(−50)	2252.628	6.74	1810.267	0.049	1569.130	0.000 75
(+12)			1968.942		1675.304	
(−12)			1969.937	1.00	1675.321	0.017
(+60)	2392.907		1977.516		1732.949	
(−60)	2397.957	5.05	1977.673	0.16	1732.952	0.002 7

rotor in the body-fixed frame (with the z axis chosen along ρ); the pertinent reduced masses are $\mu_1^{-1}=m_F^{-1}+(2m_H)^{-1}$ and $\mu_2=m_H/2$. An explicit expression for H_{VR} is given by Tennyson and Sutcliffe.[32]

It is clear from Eq. (4) that although the potential V is two-dimensional, we have to diagonalize a five-dimensional Hamiltonian similar to that previously treated by Nesbitt and Naaman[3] for ''hinge'' and ''pinwheel'' floppy triatomics. The Coriolis coupling between the external (α, β, γ) and hindered-internal rotation (θ) in H_{VR} is what makes the problem five-dimensional.

The wave function of a state with *total* angular momentum J and projection onto the space-fixed Z axis M can be written as in Ref. 30,

$$\Psi_{JM}=\sum_{K,l} \Psi_{JlK}(R)\cdot P_{lK}(\cos\,\theta)\cdot D^J_{MK}(\alpha,\beta,\gamma), \tag{5}$$

where the $D^J_{MK}(\alpha,\beta,\gamma)$ are the well known rotation matrix elements,[33] and the $P_{lK}(\cos\,\theta)$ are the normalized associated Legendre polynomials. The $\Psi_{JlK}(R)$ are the vibrational (or scattering) wave functions for the channel labeled by quantum numbers J,l,k.

For $J=0$, the wave function (5) is independent of the Euler angles and the H_{VR} term in Eq. (4) can be omitted. In this case, numerical diagonalization of the Hamiltonian (4) was performed using an orthogonal basis of 40 harmonic oscillator wave functions $v(\rho)$ spanning the R-coordinate and 40 Legendre polynomials $P_{lK}(\cos\,\theta)$ for the θ variable. An absolute precision of 10^{-6} cm^{-1} is achieved for the lowest energy level, but the precision drops to 10^{-4} cm^{-1} for the highest bound level supported by the potential of Eq. (1).

For $J\neq 0$, the matrix elements of the Hamiltonian (4) $\langle J,M,l',K'|H_0+H_{VR}|J,M,K,l\rangle$ among the basis states $P_{lK}D^J_{MK}$ used in constructing the wave function (5) have been calculated by Tennyson and Sutcliffe,[32] and found to be

$$\langle l'K'|H_0|Kl\rangle=\delta_{K'K}\delta_{l'l}\left\{-\frac{\hbar^2}{(2\mu_1\rho^2)}\frac{\partial}{\partial\rho}\left(\rho^2\frac{\partial}{\partial\rho}\right)-\hbar^2 l(l+1)\left[\frac{1}{(2\mu_1\rho^2)}+\frac{1}{(2\mu_2 r_e^2)}\right]\right\}+\delta_{KK'}\langle l'K|V(\rho,\theta)|lK\rangle, \tag{6a}$$

$$\langle l'K'|H_{VR}|lK\rangle=\frac{\hbar^2}{(2\mu_1\rho^2)}\{-\delta_{K'K+1}\delta_{l'l}C^+_{JK}C^+_{lK}-\delta_{K'K-1}\delta_{l'l}C^-_{JK}C^-_{lK}+\delta_{K'K}\delta_{l'l}\times[J(J+1)-2K^2]\}^{1/2}, \tag{6b}$$

where $C^{\pm}_{JK}=[J(J+1)-K(K\pm 1)]^{1/2}$.

For $J=1$, the wave function (5), which has fixed values of J and M, is a sum of three terms having $K=0,\ \pm 1$. The diagonalization required to find the eigenvalues of H has been performed in two steps. First, blocks of the H matrix with $K=K'=0,\ \pm 1$ were *separately* diagonalized using basis sets of 40 harmonic oscillator wave functions $v(\rho)$ and 41 associated Legendre polynomials $P_{lK}(\cos\,\theta)$ for each K. Subsequently, the resultant approximate wave functions Ψ, each having fixed K, were used as a basis for diagonalization of the total matrix that includes the nondiagonal interaction $\langle K|K'\rangle$ detailed in Eq. (6b). We found that a precision of 10^{-6} cm^{-1} is achieved when 20 such basis functions Ψ for $K=0,\ \pm 1$ are used.

The results of our calculation for $J=0$ are given in Table III (with energies measured from the minimum of the PES). The tunneling doublets for successive n values are approximately spaced by the vibrational quantum along the ρ coordinate. Since the equilibrium configuration of $H_2 \cdot F^-$ is linear, n can be associated with the longitudinal quantum number for small oscillations along the axis of the complex. The tunneling splitting is seen to grow with n from 0.029

TABLE IV. Energies (E,cm^{-1}) of the vibration-tunneling states in $H_2 \cdot F^-$, $D_2 \cdot F^-$, and $T_2 \cdot F^-$ for the case $J=1$ with (K-doubled spectra) and without ($|K|=0,1$) Coriolis forces.

Species	$K=0$		$K=1$		K-doubled	
$H_2 \cdot F^-$	$(+/-,n,\nu)$	E	$(+/-,n,\nu)$	E	$(+/-,n,\nu)$	E
	(+00)	987.2243			(+00)	987.2207
	(−00)	987.2535			(−00)	987.2499
	(+10)	1300.9879			(+10)	1300.9760
	(−10)	1301.1136			(−10)	1301.1016
	(+20)	1591.7727			(+20)	1591.7536
	(−20)	1592.1885			(−20)	1592.1691
			(+01)	1738.4305	(+01)	1738.4305
					(+01)	1738.4321
			(−01)	1739.7086	(−01)	1739.7086
					(−01)	1739.7095
	(+30)	1854.1320			(+30)	1854.1084
	(−30)	1855.3700			(−30)	1855.3448
			(+11)	2012.6370	(+11)	2012.6370
					(+11)	2012.6382
			(−11)	2017.5245	(−11)	2017.5183
					(−11)	2017.5245
	(+40)	2087.1328			(+40)	2087.1088
	(−40)	2089.9941			(+40)	2089.9665
			(+21)	2248.5613	(+21)	2248.5613
					(+21)	2248.5662
			(−21)	2262.9973	(−21)	2262.9637
					(−21)	2262.9973
$D_2 \cdot F^-$	(+00)	722.8836			(+00)	722.8820
	(−00)	722.8837			(−00)	722.8821
	(+10)	965.4826			(+10)	965.4771
	(−10)	965.4829			(−10)	965.4774
	(+20)	1197.4660			(+20)	1197.4367
	(−20)	1197.4472			(−20)	1197.4379
			(+01)	1286.9688	(+01)	1286.9688
					(+01)	1286.9700
			(−01)	1286.9722	(−01)	1286.9722
					(−01)	1286.9733
	(+30)	1417.3679			(+30)	1417.3551
	(−30)	1417.3722			(−30)	1417.3594
			(+11)	1513.5917	(+11)	1513.5917
					(+11)	1513.5921
			(−11)	1513.6107	(−11)	1513.6107
					(−11)	1513.6111
	(+40)	1623.5313			(+40)	1623.5157
	(−40)	1623.5457			(−40)	1623.5300
			(+21)	1726.8367	(+21)	1726.8363
					(+21)	1726.8367
			(−21)	1726.9132	(−21)	1726.9127
					(−21)	1726.9132
	(+02)	1765.2399			(+02)	1765.2384
	(−02)	1765.4357			(−02)	1765.4340
	(+50)	1816.4091			(+50)	1816.3915
	(−50)	1816.4476			(−50)	1816.4300
$T_2 \cdot F^-$	(+00)	601.4944			(+00)	601.4934
	(−00)	601.4944			(−00)	601.4934
	(+10)	811.4995			(+10)	811.4958
	(−10)	811.4995			(−10)	811.4958
	(+20)	1014.2535			(+20)	1014.2470
	(−20)	1014.2535			(−20)	1014.2470
			(+01)	1073.0643	(+01)	1073.0643
					(+01)	1073.0632
			(−01)	1073.6544	(−01)	1073.6544
					(−01)	1073.6536
	(+30)	1209.0316			(+30)	1209.0226
	(−30)	1209.0317			(−30)	1209.0226
			(+11)	1272.7340	(+11)	1272.7340
					(+11)	1272.7346
			(−11)	1272.7342	(−11)	1272.7342

TABLE IV. (*Continued*.)

Species	$K=0$		$K=1$		K-doubled
				(−11)	1272.7348
(+40)	1394.9344			(+40)	1394.9230
(−40)	1394.9346			(−40)	1394.9232
		(+21)	1463.8455	(+21)	1463.8455
				(+21)	1463.8457
		(−21)	1463.8466	(−21)	1463.8466
				(−21)	1463.8468
(+02)	1489.3696			(+02)	1489.3688
(−02)	1489.3721			(−02)	1489.3713
(+50)	1571.3061			(+50)	1571.2928
(−50)	1571.3068			(−50)	1571.2935

cm^{-1} ($n=0$) to 6.74 cm^{-1} ($n=5$), demonstrating the strong promoting effect of this longitudinal mode. Moreover, excitations of the bending mode, even to its lowest excited state, produces an even larger growth in the splitting (to ~37 cm^{-1}).

Small oscillations about the minimum along the θ coordinate correspond to the two transverse doubly degenerate bending modes whose quantum number is denoted ν, which can only be even for the $J=0$ case. The lower (upper) level in each R,θ tunneling doublet is labeled with a plus (minus) sign reflecting the wave function's parity with respect to $\theta \rightarrow \theta+\pi$. States with $\nu>2$ lie near dissociation, and are not included in Table IV.

For $J=1$ (Table IV), the matrix elements of the Hamiltonian (4) $\langle J,M,K=0,|H|,K'=1,J,M\rangle$ are much smaller than the diagonal matrix elements, [see Eqs. (6)], their ratio being roughly proportional to $m\rho/mR \cong 0.02$. For this reason, K can be approximately considered as a good quantum number, if Coriolis forces are neglected. Upon the inclusion of Coriolis terms, the $K=\pm 1$ degeneracy is removed (the so-called, K-doubling phenomenon[34]) as is clear from Table IV, where the exact results of diagonalization for $J=1$ are presented. Note, however, that K-doubling does not affect the tunneling splittings because of the symmetry of the rotation problem under the transformation $\theta \rightarrow \theta+\pi$.

Along with the eigenvalues of the Hamiltonian (4), diagonalization provides us with the wave functions of the system. This allows us to define the transition state of the system in terms of the maximum (maxima) of the wave function at the dividing line $\theta=\pi/2$, a definition previously introduced by Shida *et al.*[35] Obviously, this transition state differs from that suggested by the topology of the PES (i.e., the saddle point). The results of such an evaluation for the case $J=0$ are presented in Fig. 3. The ground state wave function at the dividing line [Fig. 3(a)] peaks at $R=2.37$ Å, far from the PES saddle point. Increasing the quantum number n of the promoting mode ρ produces additional maxima in the wave function. For $n=1$, the wave function peaks at $R=2.57$ Å and $R=1.97$ Å [Fig. 3(b)]; the absolute maximum ($R=2.57$ Å) shifts towards the saddle point, while the secondary maximum is strongly suppressed because the potential increases sharply for small ρ. Because the topology of the PES remains unchanged in passing to $D_2 \cdot F^-$ or $T_2 \cdot F^-$, the appearance of the wave functions for them is analogous to those discussed above for H_2F^-.

The Hamiltonian and the numerical procedure for calculating the spectra of the symmetrical isotopically substituted species D_2F^- and T_2F^- are identical to those discussed above for H_2F^-. The corresponding results are given in Tables III (for $J=0$) and IV (for $J=1$). The primary observation to be made for the $J=0$ spectra is that the tunneling splitting decreases dramatically [by 3 ($D_2 \cdot F^-$) and 4 ($T_2 \cdot F^-$) orders of magnitude] when moving from the $H_2 \cdot F^-$ to D_2F^- and T_2F^-. The pronounced isotope effect is due to the very high barriers that are present even at the saddle point.

B. $HD \cdot F^-$, $HT \cdot F^-$, and $DT \cdot F^-$

The potential for the mixed isotopomers given by Eq. (2) is asymmetric. As a result, the vibrational frequencies ω in the wells near $\theta=0$ and π are 884 cm^{-1} and 653 cm^{-1} for $HD \cdot F^-$, 879 cm^{-1} and 548 cm^{-1} for $HT \cdot F^-$, and 628 cm^{-1} and 526 cm^{-1} for $DT \cdot F^-$. Moreover the wells are of unequal depth at $\theta=0$ and $\theta=\pi$, with the energy difference between the potential minima being 23.3195, 80.1891, 4.9879 cm^{-1} for $HD \cdot F^-$, $HT \cdot F^-$, and $DT \cdot F^-$, respectively. Because we observed no accidental degeneracies between the levels arising from the wells near $\theta=0$ and $\theta=\pi$, there can exist no tunneling splitting, as a result of which there are two independent eigenvalue ladders, one for each well (Fig. 4). The results of our calculations of the spectra for $J=0$ are presented in Table V, where the levels are measured from the bottom of the deepest well (at $\theta=\pi$).

V. INCOHERENT TUNNELING IN $H_2 \cdot F^-$

State specific coherent tunneling and the associated vibration–rotation-tunneling spectra considered above pertain to gas phase conditions. An alternative experimentally realized situation involves an impurity molecule embedded in a chemically inert solid matrix for which interaction with the ''heat bath'' destroys the coherence of tunneling. In such cases, quantum levels in the reactant well acquire widths which give rise to a rate constant for intramolecular rearrangement instead of a tunneling splitting.

Let us consider such incoherent tunneling in $H_2 \cdot F^-$ within a model that assumes that end-over-end rotation of the

TABLE V. Spectra of mixed isotopomers $HD \cdot F^-$, $HT \cdot F^-$, and $DT \cdot F^-$ for $J=0$. Symbols 0 and π show to ladder in which well (at $\theta=0$ or π) the level belongs.

	$HD \cdot F^-$ E	$HT \cdot F^-$ E	$DT \cdot F^-$ E
π	823.100	753.716	643.229
0	921.690	944.574	685.554
π	1095.532	1003.908	866.715
0	1194.495	1192.392	908.021
π	1356.160	1244.331	1081.8878
0	1453.307	1429.981	1123.090
π	1598.531	1473.727	1287.753
0	1696.315	1656.393	1328.896
π	1822.589	1690.298	1483.056
0	1921.337	1870.570	1524.342
π	2027.254	1891.164	1665.522
0	2126.213	2070.503	1707.878

complex in the solid is frozen. Moreover, the low frequency bending vibrations of the linear complex will be incorporated in the ''bath'' degrees of freedom. The heavy fluorine atom is allowed to oscillate only along the space-fixed axis, R, connecting the F to the center of mass of H_2. The only rotation that is treated is the nearly free rotation of the small rigid H_2 rotor about the axis of oscillation of the F atom. As a result, three coordinates are required to describe the reaction system.

The rate of multidimensional tunneling can be related to the imaginary part of the free energy F of the system,[5]

$$K = 2\beta^{-1}\ \mathrm{Im}\ Z/\mathrm{Re}\ Z = \mathrm{Im}\ F, \tag{7}$$

where Z is the partition function and $\beta=\hbar/k_B T$ is the inverse temperature. This expression enables one to use the path integral expression for the partition function due to Feynmann,[36]

$$Z = \mathrm{Tr}[\exp(-\beta H)] = \int D[\mathbf{Q}(\tau)]\exp\{-S_E[\mathbf{Q}(\tau)]\},$$
$$\mathbf{Q}(0) = \mathbf{Q}(\beta), \tag{8}$$

where the path integral sums all the periodic paths of the system connecting points $\mathbf{Q}(0)$ and $\mathbf{Q}(\beta)$ $S_E[\mathbf{Q}(\tau)]$ is the Euclidean action along the path,

$$S_E[\mathbf{Q}(\tau)] = \int_0^\beta d\tau H(\mathbf{Q}, d\mathbf{Q}/d\tau) \tag{9}$$

and H is the classical Hamiltonian of the system.

We are now required to look for the stationary points of the path integral (8); in so doing, we find trajectories that minimize the Euclidean action (9) and, thus, obey the classical equations of motion in the inverted potential $-V$ with the set of periodic boundary conditions $\theta(\tau+\beta)=\theta(\tau)$. The nontrivial solutions to these equations have been characterized as instantons. In one dimension, such solutions were extensively studied by Langer,[37] Callan and Coleman,[38] and Polyakov.[39]

It follows from Eqs. (7) and (8), that the instanton action S determines the incoherent tunneling rate as

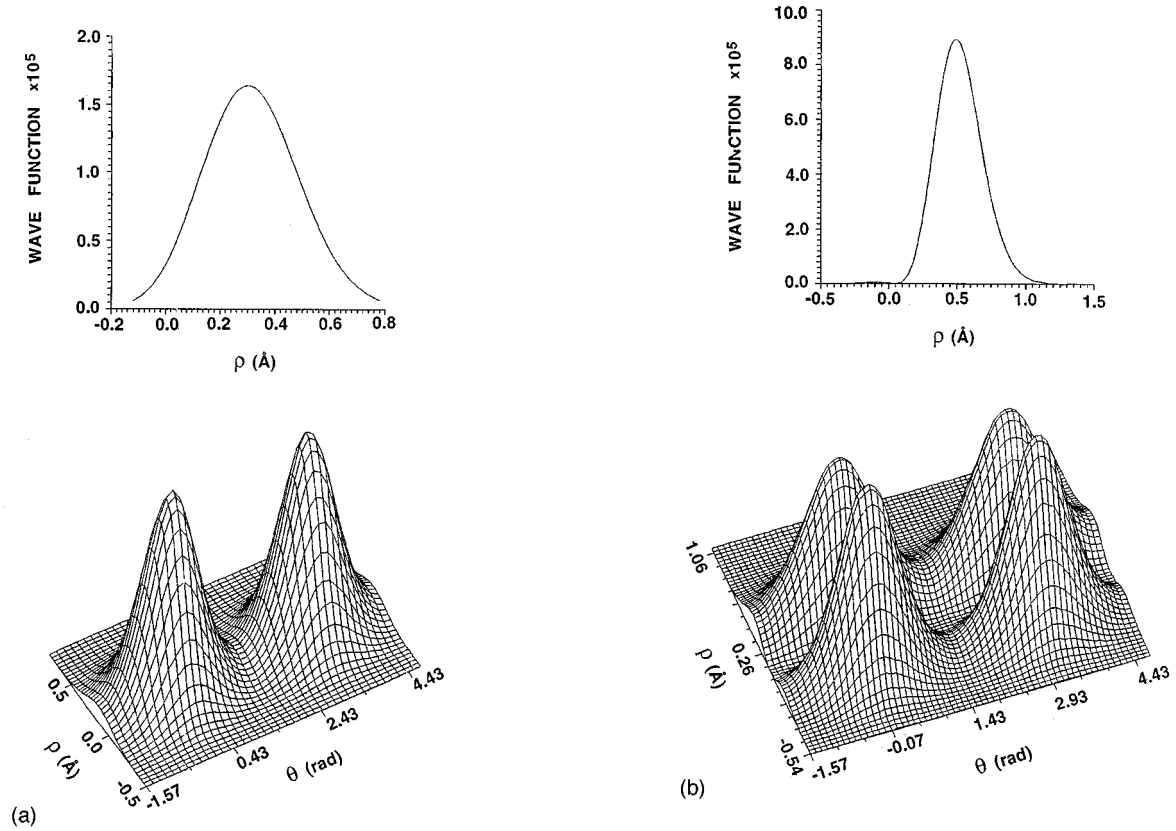

FIG. 3. Scaled two-dimensional wave functions $\Psi(\rho,\theta)$ for the ground (+00) (a) and first vibrationally excited (+10)(b) states of the $H_2 \cdot F^-$ complex in the rotational state $J=0$. Section of the wave function $\Psi(\rho,\theta)$ in the dividing line $\theta=\pi/2$ are shown in insets.

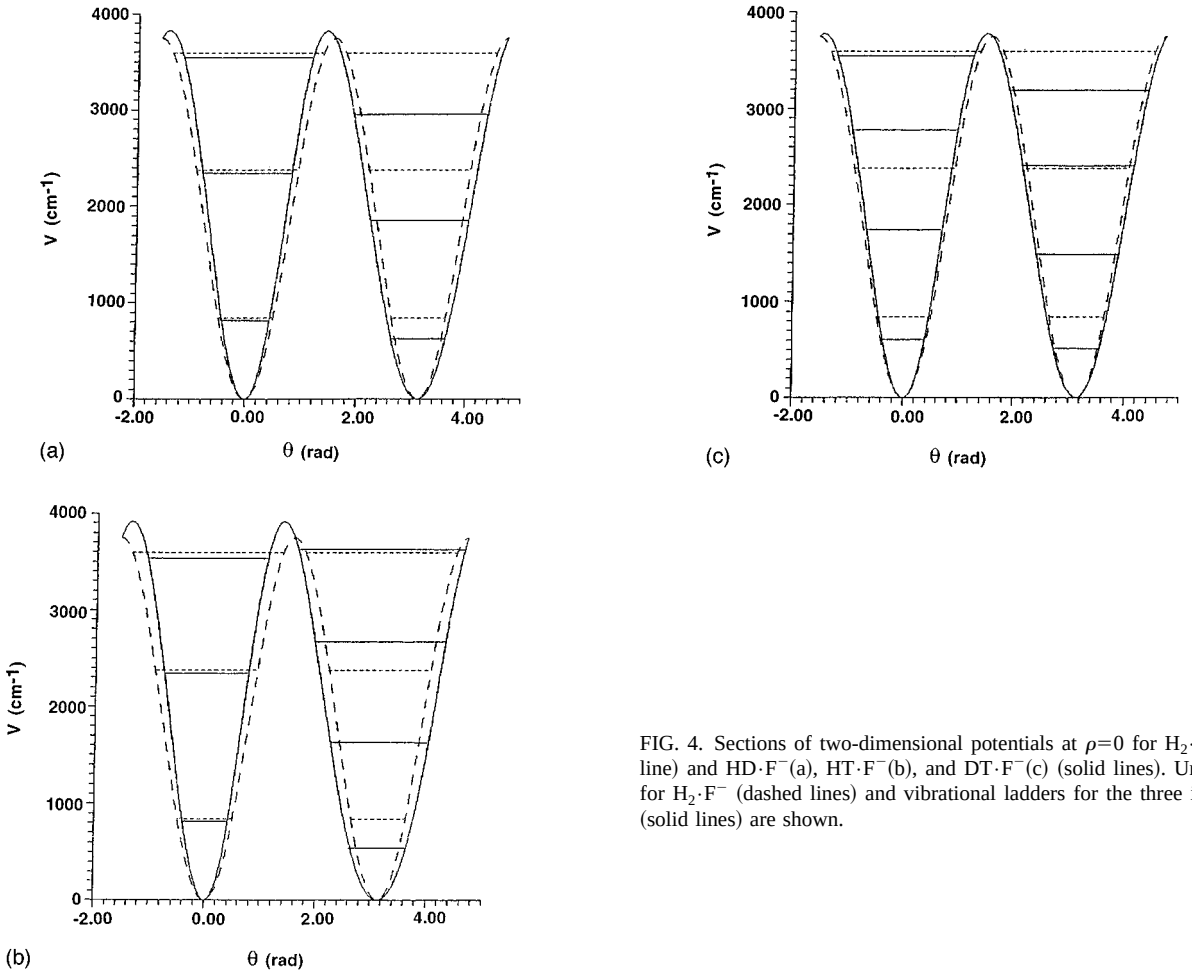

FIG. 4. Sections of two-dimensional potentials at $\rho=0$ for $H_2 \cdot F^-$ (dashed line) and $HD \cdot F^-$(a), $HT \cdot F^-$(b), and $DT \cdot F^-$(c) (solid lines). Unsplit levels for $H_2 \cdot F^-$ (dashed lines) and vibrational ladders for the three isotopomers (solid lines) are shown.

$$K(\beta) \propto \exp(-S_{\text{ins}}). \tag{10}$$

The main feature of multidimensional instantons is that, unlike the well-known one-dimensional variants, the shape of the optimal trajectory changes with temperature. Expression (10) allows the determination of a transition state for incoherent tunneling as a point at the dividing line through which the instanton passes. Calculation of transition state geometries at different temperatures thus becomes an important goal. Then we can compare these results to evolution of the transition state with changing quantum number in the coherent problem described above.

The semiclassically exact expression for $K(\beta)$ additionally includes several factors.[5]

(1) A longitudinal prefactor, associated with the invariance of the instanton with respect to time shift.
(2) A transverse prefactor, stemming from Gaussian fluctuations around the instanton trajectory and determining the width of the "tunneling channel."[40]

Note, that the rate constant should also be dependent on the spectral density of the coupling coefficients describing the interaction between the reaction complex and bath.[5] It is essential, however, that until the crossover temperature from Arrhenius activated to tunneling regimes is smaller than the Debye temperature, which is commonly the case,[5] this spectral function has no effect on the temperature behavior of the rate constant.

The numerical procedure for calculating the transverse prefactor, which, for three-dimensional problems depends on four stability parameters of the instanton trajectory,[5] is well developed.[7,41,42] Its inclusion into the expression for the rate constant becomes crucial when the stability parameters of instanton approach zero, signaling tunneling path bifurcation. This phenomena is normally due to the existence of two or more equivalent saddle points on the PES.[31] For the problem in question, however, the topology of the PES suggests no bifurcations of the instanton. Thus, all the information on the evolution of the transition-state geometry can be extracted from the instanton solution itself, contributing to $K(b)$ according to Eq. (10).

The instanton path satisfies the Euler–Lagrange equations, which in spherical coordinates (R,θ,φ) read

$$\mu_1 d^2R(\tau)/d\tau^2 = \partial V(R,\theta)/\partial R, \tag{11a}$$

$$\mu_2 d^2\theta(\tau)/d\tau^2 = \partial V(R,\theta)/\partial\theta + \mu_2 \sin\theta \cos\theta \dot{\varphi}^2, \tag{11b}$$

$$d[\sin^2\theta(\tau)\dot{\varphi}(\tau)]/d\tau = 0, \tag{11c}$$

with the following boundary conditions

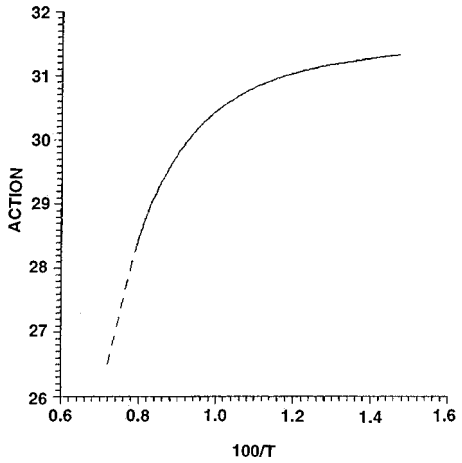

FIG. 5. Calculated temperature dependence of instanton action Eq. (9). Dashed line (for $T<125$ K) corresponds to the Arrhenius region.

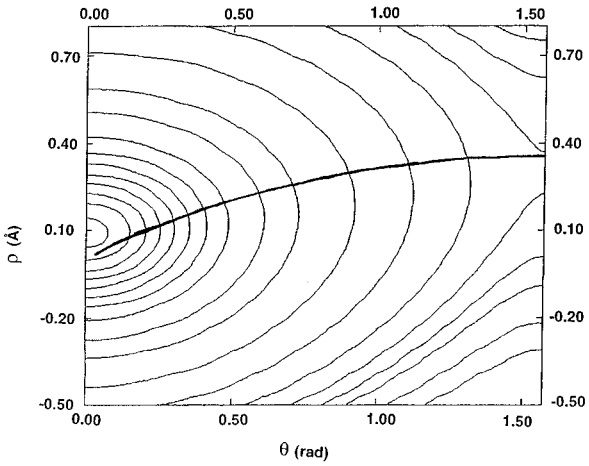

FIG. 6. Cut through the wave function $\Psi(\rho,\theta)$ of the $H_2 \cdot F^-$ complex in the ground vibrational state (00) (for $J=0$) and instanton trajectory for $T=20$ K.

$$R(\tau+\beta)=R(\tau);$$
$$\theta(\tau+\beta)=\theta(\tau); \tag{11d}$$
$$\varphi(\tau+\beta)=\varphi(\tau).$$

This trajectory becomes extreme, when

$$\dot{\varphi}=0 \tag{11e}$$

and the tunneling motion is two dimensional, being confined to the (R,θ) plane.

The results of numerical integration of Eqs. (11) are shown in Fig. 5. The instanton action (Fig. 5) achieves a low-temperature plateau below $T=70$ K. The crossover temperature β_0 at which the probability of an overbarrier transition equals that for underbarrier tunneling, equals 125 K. At this temperature, the instanton appears near the saddle point, so that

$$\beta_0=\omega^{\#}/2\pi, \tag{12}$$

where $\omega^{\#}$ is the imaginary frequency at the saddle point. Equation (12) reflects the fact that instanton period cannot be smaller than the period of oscillation in the inverted potential near the saddle point. The temperature evolution of tunneling trajectories in the (R,θ) plane is illustrated in Fig. 2. For $\beta<\beta_0$, the instanton ''sits'' at the saddle point with the action $S=\beta V^{\#}$, and the Arrhenius dependence of the rate constant $k=\exp(-\beta V^{\#})$ holds. With decreasing temperature $\beta>\beta_0$, the instanton gradually elongates and moves away from the MEP. The lower the temperature, the shorter the distance R in the T-shaped transition state of complex to the equilibrium position in the linear complex. Finally, we see that the temperature behavior of the transition state geometry for incoherent transitions is very similar to that for coherent tunneling described above.

According to the well-known Herring's formula,[43] the tunneling splitting Δ can be expressed in the form of the integral of the probability flux $\Psi\Delta\Psi^*$ over the dividing line. As was shown by Schmid,[44] the underbarrier wave function of the ground state is determined by the action along the tunneling trajectory, starting from the potential minimum and coinciding with the instanton trajectory with infinite period (zero temperature). In this connection, one might expect that instanton with $\beta\rightarrow(\infty)$ should intersect the dividing line $\theta=\pi/2$ in the vicinity of maximum of the ground state wave function. This is actually the case, as seen from the contour plot of the wave function in Fig. 6. It is noteworthy that maxima of wave functions at the dividing line $\theta=\pi/2$ for higher n levels as well as the instanton path for increasing temperature shift towards the saddle point in tandem. This behavior reflects the contribution of higher vibrational states to the statistically averaged tunneling rate constant.

VI. CONCLUSION

The complex H_2F^- is an illustrative example of a tunneling system for which no reduction procedure[5] is necessary to elucidate the tunneling dynamics. In this work, we start by calculating the three dimensional *ab initio* PES, we then fit our *ab initio* data to a reasonable and flexible functional form. Then, we determine the vibrational–rotation-tunneling spectra and analyze the wave functions of different vibrationally excited levels. This anion complex is especially attractive because the potential wells are rather deep, so the vibrational progressions are long and the variation of the tunneling splitting within such progressions can be easily followed. H_2F^- is thus distinct from, for example, malonaldehyde or the hydroxyoxalate anion,[5] in which the wells are so shallow that the vibrational progressions have only one or two levels below the barrier.

In our study of coherent (has-phase) tunneling, we found that the $H_2\cdots F^-$ intermolecular vibration promotes tunneling, and that the tunneling splitting grows by a factor of 150 within the progression of this mode. Moreover, excitation of the bending mode by two quanta causes the splittings to grow by more than three orders of magnitude. This is due to the topology of the PES for H_2F^-[5–8] which can be clarified by examining contributions from various tunneling paths. The optimal tunneling path can be thought of as involving a compromise between two factors, the *length* of path and the

barrier height along the path. Since the barrier along θ for frozen R is 3.6 kcal/mol higher than the saddle point, the ''sudden'' path $\rho=0$ is highly improbable. At the same time, since the minimum-energy path (MEP) is significantly curved, the adiabatic limit, corresponding to an effective one-dimensional vibrationally adiabatic potential, cannot be achieved either. Hence, the most effective trajectories lie in the intermediate region between the adiabatic and ''sudden'' paths. With increasing quantum number in the ρ mode, the extreme path becomes shorter and approaches the MEP. Because there is no reorganization along ρ coordinate, this leads to an increase in the tunneling splitting.

Studying the spectra of states with total angular momentum $J=1$, we found that although rotation of the complex as a whole shifts the vibrational ladders in the wells, it has almost no affect on the tunneling splittings. An influence appears only for the heavier isotopomers D_2F^- and T_2F^-, in which K doubling is comparable or greater in magnitude than the tunneling splitting.

Along with these studies of coherent tunneling in H_2F^-, we also calculated the probability of incoherent tunneling transitions using a model in which emphasis is placed on intermolecular vibration and tunneling rotation with coupling to the environment destroying the coherence. Within this model, we are able not only to follow the temperature dependence of the rate constant of tunneling in H_2F^-, but also to compare qualitatively the dynamics of the coherent and incoherent transitions.

The most valuable characteristic is shown to be the geometry of the transition state. It is found that the maxima of the wave functions at the dividing line shift towards the saddle point with increasing quantum number of the promoting mode in much the same fashion as the instanton trajectories approach the MEF with increasing temperature.

We hope that our work will lend impetus to experimental studies of the tunneling spectra of H_2F^-. Data from such studies would allow one to estimate the accuracy with which the PES is obtained and to determine how errors in the PES in the regions far from equilibrium affect the resulting tunneling spectra and dynamics.

ACKNOWLEDGMENTS

This work was supported by the Office of Naval Research and by the National Science Foundation, Grant No. CHE9116286, and by Russian Fund of Fundamental Investigations, Grant No. 93-03-5930.

[1] (a) J. Z. H. Zhang, W. H. Miller, A. Weaver, and D. Neumark, Chem. Phys. Lett. **182**, 283 (1991); (b) S. E. Bradforth, D. W. Arnold, D. M. Neumark, and D. E. Manolopoulos, J. Chem. Phys. **99**, 6345 (1993); (c) D. M. Neumark, Acc. Chem. Res. **26**, 33 (1993).
[2] J. A. Nichols, R. A. Kendall, S. J. Cole, and J. Simons, J. Phys. Chem. **95**, 1074 (1991).
[3] D. J. Nesbitt and R. Naaman, J. Chem. Phys. **91**, 3801 (1989).
[4] V. A. Benderskii and V. I. Goldanskii, Int. Rev. Phys. Chem. **11**, 1 (1992).
[5] V. A. Benderskii, D. E. Makarov, and C. A. Wight, *Chemical Dynamics at Low Temperatures* (Wiley, New York, 1994).
[6] V. A. Benderskii, V. I. Goldanskii, and D. E. Makarov, Chem. Phys. **159**, 29 (1992).
[7] V. A. Benderskii, S. Yu. Grebenshchikov, E. V. Vetoshkin, G. V. Mil'nikov, and D. E. Makarov, J. Phys. Chem. **98**, 3300 (1994).
[8] V. A. Benderskii, S. Yu. Grebenshchikov, G. V. Mil'nikov, and E. V. Vetoshkin, Chem. Phys. (submitted).
[9] (a) T. R. Dyke, K. M. Mack, and J. S. Muenter, J. Chem. Phys. **66**, 498 (1977); (b) L. H. Coudert, F. J. Lovas, R. D. Suenram, and J. T. Hougen, *ibid*. **87**, 6290 (1987); (c) J. A. Odutola, T. A. Hu, D. Prinslow, S. E. O'dell, and T. R. Dyke, *ibid*. **88**, 5352 (1988); (d) L. Martinache, S. Jans-Burli, B. Vogelsanger, and A. Bauder, Chem. Phys. Lett. **149**, 424 (1988); (e) K. L. Busarow, R. C. Cohen, G. A. Blake, K. B. Laughlin, Y. T. Lee, and R. J. Saykally, J. Chem. Phys. **90**, 3937 (1989); (f) G. T. Fraser, R. D. Suenram, and L. H. Coudert, *ibid*. **90**, 6077 (1989); (g) G. T. Fraser, R. D. Suenram, L. H. Coudert, and R. S. Frye, J. Mol. Spectrosc. **137**, 244 (1989); (h) T. A. Hu, and T. R. Dyke, J. Chem. Phys. **91**, 7348 (1990); (i) E. Zwart, J. J. ter Meulen, and W. L. Meerts, Chem. Phys. Lett. **166**, 500 (1990); (j) G. T. Fraser, Int. Rev. Phys. Chem. **10**, 189 (1991); (k) N. Pugliano and R. J. Saykally, J. Chem. Phys. **96**, 1832 (1992).
[10] N. Pugliano, and R. J. Saykally, Science **257**, 1937 (1992).
[11] (a) M. J. Howard, S. Burdenski, C. F. Giese, and W. R. Gentry, J. Chem. Phys. **80**, 4137 (1984); (b) D. D. Nelson, Jr., G. T. Fraser, and W. Klemperer, *ibid*. **83**, 6201 (1985); (c) G. T. Fraser, D. D. Nelson, Jr., A. C. Charo, and W. Klemperer, *ibid*. **82**, 2535 (1985); (d) D. D. Nelson, W. Klemperer, G. T. Fraser, F. J. Lovas, and R. D. Suenram, *ibid*. **87**, 6364 (1987); (e) J. G. Loeser, C. A. Schmuttenmaer, R. C. Cohen, M. J. Elrod, D. W. Steyert, R. J. Saykally, R. E. Bumgarner, and G. A. Blake, *ibid*. **97**, 4727 (1992).
[12] (a) T. R. Dyke, B. J. Howard, and W. Klemperer, J. Phys. Chem. **56**, 2442 (1972); (b) W. J. Lafferty, R. D. Suenram, and F. J. Lovas, J. Mol. Spectrosc. **123**, 434 (1987); (c) K. von Puttkamer, M. Quack, and M. A. Suhm, Mol. Phys. **65**, 1025 (1988).
[13] (a) G. A. Blake, K. L. Busarow, R. C. Cohen, K. B. Laughlin, Y. T. Laughlin, Y. T. Lee, and R. J. Saykally, J. Chem. Phys. **89**, 6577 (1988); (b) G. A. Blake and R. E. Bumgarner, *ibid*. **91**, 7300 (1989).
[14] T. R. Dyke, *Topics in Current Chemistry* (Springer, New York, 1984), Vol. 120, p. 85.
[15] G. T. Fraser, D. D. Nelson, Jr., A. C. Charo, and W. Klemperer, J. Chem. Phys. **82**, 2535 (1985).
[16] H. W. Crofton, M.-F. Jagod, B. D. Rehfuss, and T. Oka, J. Chem. Phys. **91**, 5139 (1989).
[17] (a) A. D. Buckingham, P. W. Fowler, and J. M. Hutson, Chem. Rev. **88**, 963 (1988); (b) D. J. Nesbitt, *ibid*. **88**, 843 (1988); (c) A. C. Legon, Chem. Soc. Rev. **19**, 197 (1990); (d) C. Cohen and R. J. Saykally, Annu. Rev. Phys. Chem. **42**, 369 (1991); (e) J. Phys. Chem. **96**, 1024 (1992); (f) Z. Bacic and J. C. Light, Annu. Rev. Phys. Chem. **40**, 469 (1989).
[18] (a) T. R. Dyke, J. Chem. Phys. **66**, 492 (1977); (b) L. H. Coudert, and J. T. Hougen, J. Mol. Spectrosc. **130**, 86 (1988); (c) J. T. Hougen, *ibid*. **137**, 244 (1989); (d) L. H. Coudert and J. T. Hougen, *ibid*. **139**, 259 (1990).
[19] J. W. I. van Bladel, A. van der Avoird, P. E. S. Wormer, and R. J. Saykally, J. Chem. Phys. **97**, 4750 (1992).
[20] (a) P. R. Bunker, T. Carrington, Jr., P. C. Gomez, M. D. Marshall, M. Kofranek, H. Lischka, and A. Karpfen, J. Chem. Phys. **91**, 5154 (1989); (b) P. R. Bunker, P. Jensen, A. Karpfen, M. Kofranek, H. Lishka, *ibid*. **92**, 7432 (1990); (c) P. Jensen and P. R. Bunker, *ibid*. **93**, 6266 (1990).
[21] J. Tennyson and S. Miller, J. Chem. Phys. **87**, 6648 (1987).
[22] (a) R. Escribano and P. R. Bunker, J. Mol. Spectrosc. **122**, 325 (1987); (b) J. T. Hougen, *ibid*. **123**, 197 (1987); (c) R. Escribano, P. R. Bunker, and P. C. Gomes, Chem. Phys. Lett. **150**, 60 (1988); (d) P. C. Gomes and P. R. Bunker, *ibid*. **165**, 351 (1990).
[23] (a) L. Ya. Baranov and A. I. Boldyrev, Chem. Phys. Lett. **96**, 218 (1983); (b) L. Ya. Baranov and A. I. Boldyrev, Mol. Phys. **54**, 989 (1985); (c) N. Ohashi and J. T. Hougen, J. Mol. Spectrosc. **153**, 429 (1992); (d) E. Hirota, *ibid*. **153**, 447 (1992).
[24] H. B. Schlegel, J. Comput. Chem. **3**, 214 (1982).
[25] M. J. Frisch, G. W. Trucks, M. Head-Gordon, P. M. W. Gill, M. W. Wong, J. B. Foresman, B. G. Johnson, H. B. Schlegel, M. A. Robb, E. S. Replogle, R. Gomperts, J. L. Anders, K. Raghavachari, J. S. Binkley, C. Gonzales, R. L. Martin, D. J. Fox, D. J. DeFrees, D. J. Defrees, J. Baker, J. J. P. Stewart, and J. A. Pople, GAUSSIAN 92, Revision C, Gaussian Inc., Pittsburgh, Pennsylvania, 1992.
[26] J. A. Pople, M. Head-Gordon, and K. Raghavachari, J. Chem. Phys. **87**, 5968 (1987).
[27] R. J. Le Roy and J. S. Carley, Adv. Chem. Phys. **42**, 353 (1980).
[28] C. Eckart, Phys. Rev. **47**, 552 (1935).
[29] C. F. Curtiss, J. O. Hirshfelder, and F. T. Adler, J. Chem. Phys. **18**, 1638 (1950).

[30] B. T. Sutcliffe, in *The Dynamics of Molecules*, NATO ASI Ser., edited by R. G. Woolley (Plenum, New York, 1980).
[31] L. C. Biedenharn and J. D. Louck, *Angular Momentum in Quantum Physics* (Addison-Wesley, Massachusetts, 1981), Vol. 2.
[32] J. Tennyson and B. T. Sutcliffe, J. Chem. Phys. **77**, 4061 (1982).
[33] J. O. Hirshfelder and E. P. Wigner, Proc. Amer. Acad. Sci. **21**, 113 (1935).
[34] C. H. Townes and A. L. Schawlow, *Microwave Spectroscopy* (McGraw-Hill, New York, 1955).
[35] N. Shida, P. F. Barbara, and J. E. Almlof, J. Chem. Phys. **91**, 4061 (1989); **94**, 3633 (1991).
[36] R. P. Feynman and A. R. Hibbs, *Quantum Mechanics and Path Integrals* (McGraw-Hill, New York, 1965).
[37] G. S. Langer, Ann. Phys. **54**, 258 (1969).
[38] C. G. Callan and S. Coleman, Phys. Rev. D **16**, 1762 (1977).
[39] A. M. Polyakov, Nucl. Phys. B **121**, 429 (1977).
[40] V. A. Benderskii, P. G. Grinevitch, D. E. Makarov, and D. L. Pastur, Chem. Phys. **161**, 51 (1992).
[41] V. A. Benderskii, S. Yu. Grebenshchikov, E. V. Vetoshkin, and D. E. Makarov, Chem. Phys. **188**, 19 (1994).
[42] V. A. Benderskii, V. I. Goldanskii, and D. E. Makarov, Chem. Phys. Lett. **186**, 517 (1991).
[43] C. Herring, Rev. Mod. Phys. **34**, 341 (1962).
[44] A. Schmid, Ann. Phys. **170**, 333 (1986).